

ACADEMIC
PRESS

Available online at www.sciencedirect.com



Journal of Molecular Spectroscopy xxx (2003) xxx–xxx

Journal of
MOLECULAR
SPECTROSCOPY

www.elsevier.com/locate/jms

Fluorescence excitation spectroscopy of the $\tilde{A}^2A_1 \leftarrow \tilde{X}^2B_1$ system of jet-cooled NH_2 in the region 2900–4300 Å

Ju Xin,^a Haiyan Fan,^b Ionela Ionescu,^b Chris Annesley,^b and Scott A. Reid^{b,*}^a Department of Physics and Engineering Technologies, Bloomsburg University, Bloomsburg, PA 17815, USA^b Department of Chemistry, Marquette University, P.O. Box 1881, Milwaukee, WI 53201-1881, USA

Received 10 September 2002; in revised form 16 December 2002

Abstract

The fluorescence excitation spectrum of the $\text{NH}_2 \tilde{A}^2A_1 \leftarrow \tilde{X}^2B_1$ system in the region 2900–4300 Å has been measured under jet-cooled conditions using a pulsed discharge source. A total of fourteen bands involving the pure bending states $(0, \nu_2', 0)$ were observed and analyzed, including 10 bands not previously measured to our knowledge. The spectra are largely free from rotational perturbations at the low N values accessed in this experiment, and the molecular constants were obtained from a least squares fit to the determined spin–rovibronic term values. The derived constants are in good agreement with theoretical predictions incorporating the effects of orbital angular momentum on the spin–rotational fine structure.

© 2003 Elsevier Science (USA). All rights reserved.

1. Introduction

The NH_2 radical holds a special place in the annals of molecular spectroscopy. The $\tilde{A}^2A_1 \leftarrow \tilde{X}^2B_1$ system was first observed in absorption by Herzberg and Ramsay [1], and the seminal work of Dressler and Ramsay [2,3] established NH_2 as the first Renner–Teller molecule. The first detailed analysis of the absorption spectrum in the 3900–8300 Å region was carried out in 1959 by Dressler and Ramsay [3], and has served as a model for subsequent studies [4–22]. In addition to its fundamental importance, NH_2 is an important intermediate in the growth of AlN and GaN films by photochemical vapor deposition [23], and emission bands of the $\tilde{A}^2A_1 \leftarrow \tilde{X}^2B_1$ system are observed in the spectra of cometary comae [24].

From a theoretical standpoint, NH_2 has also received extensive scrutiny [25–43], with early studies by Pople et al. [25] and Dixon [26]. Aiming at a more quantitative understanding, Jungen et al. [29,30] fit the observed vibrational and K -type rotational levels to a Hamiltonian incorporating the effects of Renner–Teller coupling and using a semi-rigid bender model to account for the large

amplitude bending motion, thereby obtaining one-dimensional potential curves for the two electronic states. In a subsequent paper [31], the effects of orbital angular momentum on the spin–rotational fine structure was examined, and calculations using as input only the potential curves, bond lengths and spin–orbit coupling constant gave results in good agreement with experiment. This work did not treat the excited stretching modes. Gabriel et al. [36] calculated three dimensional potential energy functions for the \tilde{A} and \tilde{X} states and used a variational approach to calculate rovibronic term values up to $\sim 20000 \text{ cm}^{-1}$. The assignment of vibrational quantum numbers was complicated by the presence of anharmonic coupling, and analysis was done in terms of Fermi polyads. Above $\sim 18000 \text{ cm}^{-1}$, it was noted that vibrational assignment was possible only for \tilde{A} state levels, particularly those involving pure bending states. The study of the Renner effect in NH_2 continues to be an area of active theoretical interest, as evidenced by the recent work of Duxbury and Alijah [40–42] and Jensen et al. [43].

We were initially motivated to study, via quantum beat spectroscopy, the Zeeman effect in the pure bending levels of the \tilde{A} state, to provide further insight into the effects of orbital angular momentum and as a prelude to the study of such effects in carbene radicals. In the

* Corresponding author. Fax: 1-414-288-7066.
E-mail address: scott.reid@mu.edu (S.A. Reid).

66 course of that work, we measured with high precision
67 the fluorescence lifetimes of 21 bands in the
68 $\tilde{A}^2A_1 \leftarrow \tilde{X}^2B_1$ system, and obtained fluorescence excita-
69 tion spectra of 14 bands involving the pure bending
70 states in the 2900–4300 Å region, 10 of which had not
71 been previously observed to our knowledge. This report
72 concerns our analysis of the latter. The results of our
73 lifetime and Zeeman measurements will be reported
74 elsewhere.

75 2. Experimental details

76 The apparatus consisted of a cubic vacuum chamber
77 evacuated by a 6 in. water-baffled diffusion pump (Var-
78 ian VHS-6), equipped with a molecular beam source and
79 fluorescence detection assembly. The NH_2 radicals were
80 generated by a pulsed electrical discharge through a
81 mixture (~1%) of NH_3 in Argon that was premixed in a
82 stainless steel cylinder. Fig. 1 shows a schematic of the
83 discharge nozzle, which featured a commercial pulsed
84 valve (General Valve Series 9, orifice diameter =
85 0.5 mm). The expansion channel diameter was 3 mm,
86 and typical backing pressure ~1 bar. The discharge was
87 initiated by an 800 V pulse of typically 15 μs duration
88 that passed through a 10 k Ω ballast resistor. The timing
89 of laser, nozzle, and discharge firing was controlled by a
90 digital delay generator (Stanford Research Systems
91 DG535), which also generated a variable width gate
92 pulse for the high voltage pulser (Directed Energy
93 GRX-1.5K-E).

94 The laser system consisted of an etalon narrowed dye
95 laser (Lambda-Physik Scanmate 2E) pumped by the
96 second or third harmonic of an injection seeded
97 Nd:YAG laser (Continuum Powerlite 7010). Wave-
98 lengths between ~320 and 375 nm were generated by

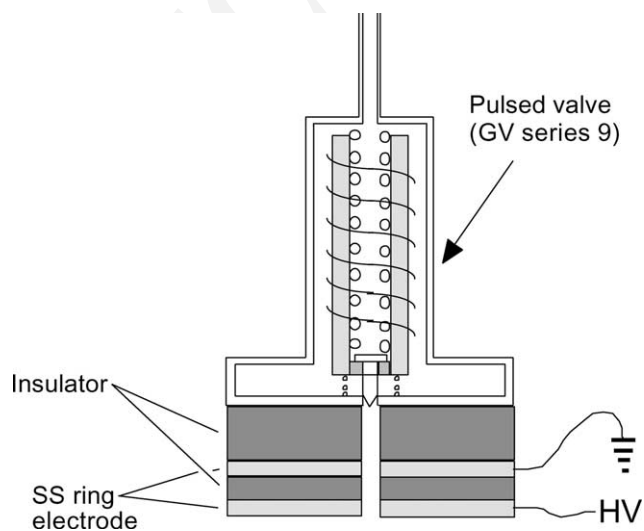


Fig. 1. Schematic of the pulsed discharge nozzle used in this work. Key: HV = high voltage.

doubling the dye laser output in a BBO crystal, while
those between ~375 and 440 nm were generated by
mixing the dye output with the Nd:YAG fundamental in
a second BBO crystal. Wavelengths between ~440 and
520 nm were generated via the use of appropriate dyes
pumped with the Nd:YAG third harmonic. The laser
beam was not focused, and typical pulse energies were
200–300 μJ in a ~3 mm diameter beam. A quartz win-
dow was used to direct a portion of the dye laser fun-
damental into a Fe–Ne lamp for absolute wavelength
calibration using the optogalvanic effect. The Nd:YAG
laser frequency (9397.44 cm^{-1}) was determined by cali-
brating the sum frequency against lines of a Fe–Ar
lamp.

These measurements utilized a mutually orthogonal
geometry of laser, molecular beam, and detector, where
the laser beam crossed the molecular beam at a distance
of ~10 mm downstream. Fluorescence was collected by
a two lens $f/2.4$ condenser assembly, and filtered via an
appropriate long-pass cutoff filter (Corion) prior to
striking a photomultiplier tube detector (Oriel) held at
typically –600 V. The PMT signal was terminated into
15 k Ω , and digitized by a fast oscilloscope (HP 54521A).
Spectral acquisition typically employed a ‘fast scan’
mode, where five laser shots were averaged in the
baseline and 20 laser shots on the peaks.

3. Results and discussion

The \tilde{A}^2A_1 state of NH_2 is quasi-linear, with a barrier
to linearity of ~730 cm^{-1} [29]. Previous authors have
utilized both linear and bent molecule formalism for the
bending levels of the \tilde{A}^2A_1 state, and the correlation
between these notations is [18]

$$v_2(\text{linear}) = 2v_2(\text{bent}) + K_a + 1. \quad (1)$$

Here we employ the linear molecule formalism. The
transition frequencies were typically determined from
fits to a Gaussian lineshape function using PSIplot
software. These frequencies were then fit using a least
squares routine to a modified form of the Hill and Van
Vleck equation [44], incorporating the well-known
ground state term values [18]. Specifically, we used Eq.
(1) of Jungen et al. [31] with the addition of a quartic
centrifugal distortion term of the form [18]

$$-D[N^2 - N_z^2]^2. \quad (2)$$

Due to the limited data set, four parameters were
typically determined for Π and Δ levels: the vibronic
term energy, T ; rotational constant, $\bar{B} [= 1/2(B + C)]$;
spin–orbit constant, A ; and asymmetry parameter,
 $q [= 1/2(B - C)]$. Three parameters were determined for
 Σ levels: T , \bar{B} , and the centrifugal distortion constant, D .
The fitting routine was tested using the extensive data set
of Dressler and Ramsay [3].

150 We obtained fluorescence excitation spectra of the Σ
151 levels $(0, v_2', 0)$, $v_2' = 17\text{--}25$, in absorption from the
152 $(0,0,0)$ $K_a = 1$ level of \tilde{X}^2B_1 . The $(0,25,0)\Sigma$ level was
153 previously observed in absorption from \tilde{X}^2B_1 $(0,2,0)$
154 $K_a = 1$ [21,22], while the $(0,17,0)\Sigma$ and $(0,19,0)\Sigma$ bands
155 were observed by Dressler and Ramsay [3]. A spectrum
156 of the $(0,23,0)\Sigma$ and $(0,23,0)\Delta$ bands is shown in Fig. 2,
157 and Table 1 lists the fit parameters determined for each
158 band. The 2_{02} level of $(0,23,0)\Sigma$ was obviously per-
159 turbed, as evidenced by the presence of an extra line in
160 all observed transitions to this state, and these were not
161 included in the fit. As shown in Table 2, our results are
162 in good agreement with previous work, with the excep-
163 tion of the vibronic term energy for $(0,17,0)\Sigma$. We cali-
164 brated the laser wavelength in this region against two
165 optogalvanic lines, and find no systematic deviation
166 between our results and those of Dressler and Ramsay
167 [3] for the Π bands, leaving the origin of this discrepancy
168 unexplained.

169 Graphs of the fitted \bar{B} and D constants vs. quanta of
170 bend (v_2') which combine our results with those of
171 Dressler and Ramsay [3] are shown in the upper and
172 lower panels, respectively, of Fig. 3. The solid line in the
173 upper panel depicts a linear fit, and with the exception of
174 $(0,15,0)\Sigma$ a relatively smooth linear dependence on v_2'
175 is found. The apparently negative centrifugal distortion
176 constants result, in the linear molecule formalism, from
177 an l -type resonance between the Σ and Δ components of
178 a vibronic level [31]. Jungen et al. [31] treated this as
179 arising from rotational asymmetry (bent molecule for-
180 malism), which to second-order gave the following ex-
181 pression:

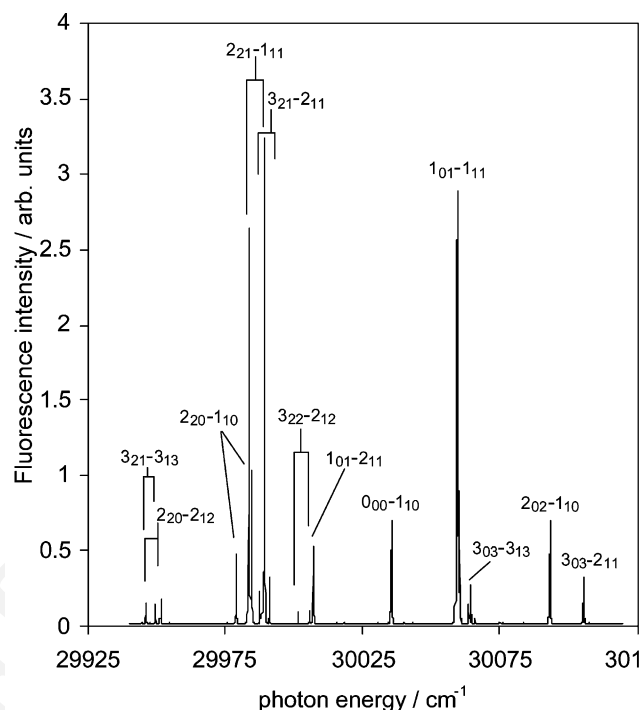


Fig. 2. Fluorescence excitation spectrum of the $(0,23,0)\Sigma$ and $(0,23,0)\Delta$ bands, with rotational assignments.

$$D_{\text{eff}} = D_{\text{cd}} - \frac{|\langle 1/2(B-C) \rangle|^2}{2\Delta E(K_a = 0 - K_a = 2)}. \quad (3)$$

In Eq. (3) D_{cd} is the contribution from centrifugal 183
distortion, $\langle 1/2(B-C) \rangle$ is the matrix element evaluated 184
between the $K_a = 0$ and $K_a = 2$ wavefunctions in the 185

Table 1
Hamiltonian parameters (in cm^{-1}) for the Σ bands measured in this work

	$(0,17,0)\Sigma$	$(0,19,0)\Sigma$	$(0,21,0)\Sigma$	$(0,23,0)\Sigma$	$(0,25,0)\Sigma$
T	24094.27(5) ^a	26 052.63(3)	28 039.83(11)	30 066.28(36)	32 115.71(21)
\bar{B}	9.243(25)	9.286(16)	9.302(46)	9.399(26)	9.505(96)
D	-0.029(2)	-0.028(1)	-0.031(3)	-0.028(20)	-0.059(7)
N^b	10	10	10	12	10
σ^c	0.05	0.03	0.11	0.28	0.18

^a One standard error given in parenthesis.

^b Number of transitions included in the fit.

^c Standard deviation of the fit.

Table 2
A comparison of the Σ band Hamiltonian parameters determined in this work with previous measurements

	$(0,17,0)\Sigma$		$(0,25,0)\Sigma$		
	This work	Ref. [3]	This work	Ref. [21]	Ref. [22]
T	24 094.27(5) ^a	24 087.8	32 115.71(21)	32 115.9(5)	32 115.9(14)
\bar{B}	9.243(25)	9.17(8)	9.505(96)	10.35(6)	10.33(18)
D	-0.029(2)	-0.024	-0.059(7)	^b	^b

^a One standard error given in parenthesis.

^b Not included in the fit.

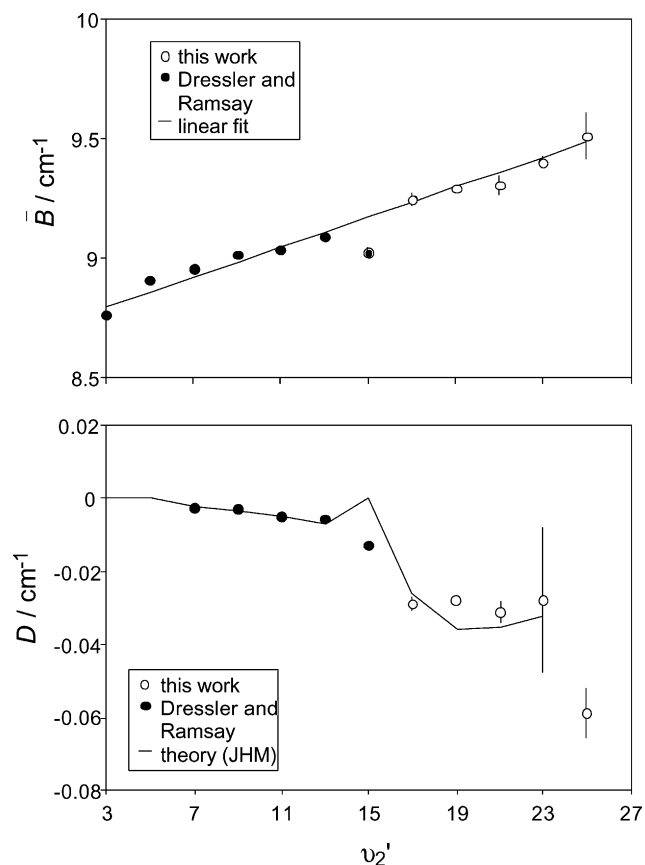


Fig. 3. Upper panel: variation of the rotational constant (\bar{B}) with quanta of bending excitation (v_2') for the Σ bands, combining our data with that of Dressler and Ramsay [3]. Lower panel: similar plot for D . The solid line marks the theoretical predictions of Jungen et al. [31].

186 \bar{A}^2A_1 state, and ΔE is the energy splitting between these
 187 states. In extending the predictions of Jungen et al. [31]
 188 to bands above (0,17,0), we used their estimate for D_{cd} ,
 189 our experimental values for ΔE , and a linear extrapo-
 190 lation of the $\langle 1/2(B - C) \rangle$ values calculated for $v_2' = 5$ –
 191 17, which apart from (0,15,0) exhibited a smooth linear
 192 dependence on v_2' . (Note that (0,15,0) Δ is in Fermi reso-
 193 nance with the (1,14,0) $K_a = 2$ level of \bar{X}^2B_1 [31].) The
 194 calculated values, shown as the solid line in the lower
 195 panel of Fig. 3, are in very reasonable agreement with
 196 experiment.

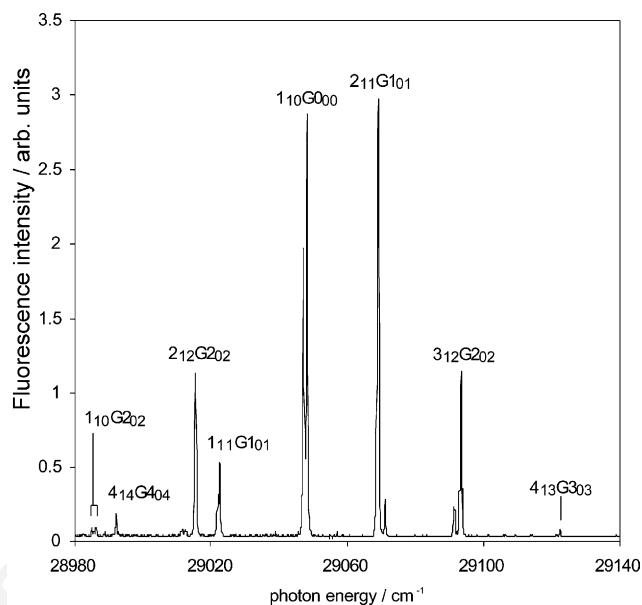


Fig. 4. Fluorescence excitation spectrum of the (0,22,0) Π band, with rotational assignments.

We obtained spectra for the Π levels (0, $v_2', 0$), 197
 $v_2' = 16$ –24, in absorption from the (0,0,0) $K_a = 0$ level 198
 of \bar{X}^2B_1 . The (0,22,0) Π band was first observed by 199
 Schliepen et al. [21], and subsequently by Chang et al. 200
 [22]. The (0,18,0) Π band and a few lines of the (0,20,0) Π 201
 band were observed by Dressler and Ramsey [3], and fit 202
 by Jungen et al. [31]. A spectrum of the (0,22,0) Π band 203
 is shown in Fig. 4, and Table 3 lists the fit parameters 204
 determined for each band. The assignment of spin–rotation 205
 components was determined unambiguously using 206
 Zeeman quantum beat spectroscopy. Scattered 207
 rotational perturbations were observed involving the 211 208
 and 414 levels of (0,22,0) Π and the 110 level of (0,24,0) Π , 209
 and transitions involving these levels were excluded 210
 from the fits. As shown in Table 4, our results are in 211
 good agreement with the previous work. 212

Graphs of the rotational constant \bar{B} , spin–orbit 213
 constant A , and asymmetry parameter q vs. quanta of bend 214
 (v_2') which combine our results with fits of the data of 215
 Ramsay and co-workers reported in [31] are shown in 216
 the upper, middle, and lower panels, respectively, of Fig. 217

Table 3
 Hamiltonian parameters (in cm^{-1}) for the Π bands measured in this work

	(0,16,0) Π	(0,18,0) Π	(0,20,0) Π	(0,22,0) Π	(0,24,0) Π
T	23109.52(97) ^a	25 049.19(9)	27 024.84(9)	29 036.13(12)	31 086.18(25)
\bar{B}	9.69(55)	9.453(14)	9.474(28)	9.668(21)	10.172(34)
A	–7.5(14)	–2.65(18)	0.28(17)	1.12(26)	0.5(5)
q	–0.15(64)	2.00(2)	2.02(3)	2.24(3)	1.70(6)
N^b	6	10	10	10	10
σ^c	0.49	0.09	0.10	0.14	0.26

^a One standard error given in parenthesis.

^b Number of transitions included in the fit.

^c Standard deviation of the fit.

Table 4
A comparison of the Π band Hamiltonian parameters determined in this work with previous measurements

	(0,18,0) Π		(0,20,0) Π		(0,22,0) Π		
	This work	Ref. [31]	This work	Ref. [31]	This work	Ref. [21]	Ref. [22]
T	25049.19(9) ^a	25050.3(4)	27024.84(9)	27025.5(15)	29036.13(12)	29035.2(2)	29036.13(7)
\bar{B}	9.453(14)	9.65(7)	9.474(28)	9.14(28)	9.668(21)	9.71(5)	9.671(6)
D	^b	0.0028(24)	^b	-0.0010(5)	^b	^b	^b
A	-2.65(18)	-2.6(7)	0.28(17)	0	1.12(26)	0.65(40)	0.93(25)
q	2.00(2)	1.865(23)	2.02(3)	1.87(30)	2.24(3)	2.14(5)	2.25(1)

^a One standard error given in parenthesis.

^b Not included in the fit.

218 5. Also shown as the solid line in each graph are the
219 theoretical predictions of Jungen et al. [31], again in
220 good agreement with experiment. The variations of
221 these parameters with v_2' clearly show the effects of or-
222 bital angular momentum. Of particular interest is the
223 variation in spin-orbit constant (A), which evidences a

224 pronounced 'saw-tooth' pattern with cycles reflecting the
225 periodic degeneracy of \tilde{X} and \tilde{A} state bending levels [31].
226 Our data show the expected damping of these effects for
227 levels far above the barrier to linearity.

228 Finally, we obtained fluorescence excitation spectra
229 for the Δ levels (0, $v_2', 0$), $v_2' = 17-23$, in absorption from
230 the (0,0,0) $K_a = 1$ level of \tilde{X}^2B_1 . To the best of our
231 knowledge these bands have not been previously ob-
232 served. A spectrum of the (0,23,0) Δ band is shown in
233 Fig. 2 above, and Table 5 lists the fit parameters deter-
234 mined for each band. Graphs of the rotational constant
235 (\bar{B}) and spin-orbit constant (A) vs. quanta of bend (v_2')

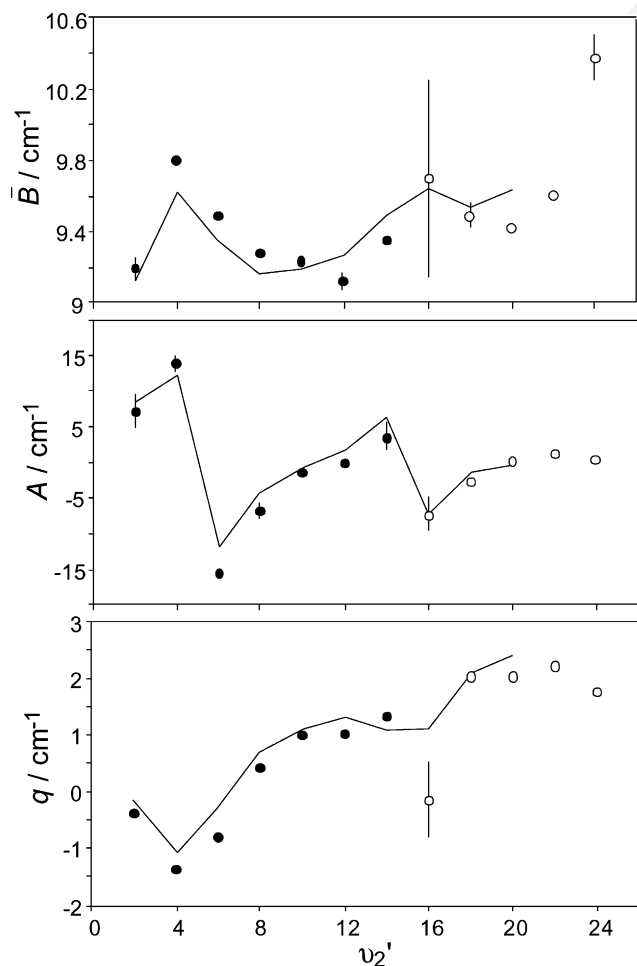


Fig. 5. Upper panel: variation of the rotational constant (\bar{B}) with quanta of bending excitation (v_2') for the Π bands, combining our data (open circles) with fits of the data of Ramsay and coworkers reported in [31]. Middle panel: similar plot for the spin-orbit constant (A). Lower panel: similar plot for the asymmetry parameter (q). The solid line in each plot marks the theoretical predictions of Jungen et al. [31].

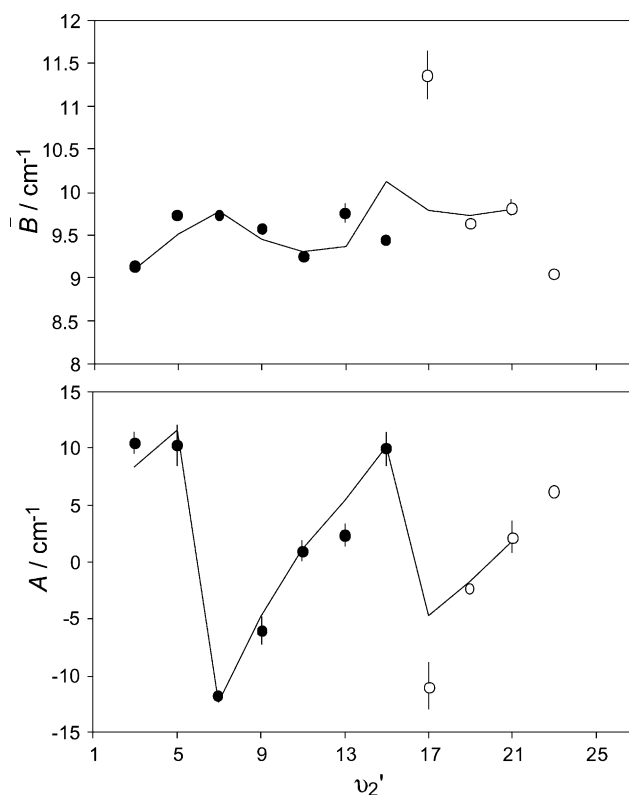


Fig. 6. Upper panel: variation of the rotational constant (\bar{B}) with quanta of bending excitation (v_2') for the Δ bands, combining our data (open circles) with fits of the data of Ramsay and coworkers reported in [31]. Lower panel: similar plot for the spin-orbit constant (A). The solid line in each plot marks the theoretical predictions of Jungen et al. [31].

Table 5
Hamiltonian parameters (in cm^{-1}) for the Δ bands measured in this work

	(0,17,0) Δ	(0,19,0) Δ	(0,21,0) Δ	(0,23,0) Δ
T	24 080.31(71) ^a	26 003.21(23)	27 978.31(61)	30 000.87(24)
\bar{B}	11.38(16)	9.640(25)	9.804(86)	9.051(53)
A	-11.5(10)	-2.37(41)	2.1(13)	6.04(52)
q	^b	0.001(2)	0.002(4)	-0.001(3)
N^c	8	10	8	12
σ^d	0.62	0.22	0.50	0.23

^a One standard error given in parenthesis.^b Fixed at 0.0 in the fit.^c Number of transitions included in the fit.^d Standard deviation of the fit.

236 which combine our results with fits of the data of
237 Ramsay and co-workers reported in [31] are shown in
238 the upper and lower panels, respectively, of Fig. 6. Also
239 shown as the solid line in each graph are the theoretical
240 predictions of Jungen et al. [31], which again are in very
241 reasonable agreement with experiment.

242 A comparison of the vibronic origins for the bands
243 measured in this work with the predictions of Jungen et
244 al. [30] is given in Table 6. The calculated values were
245 derived from a least squares fit of the potential param-
246 eters to all available experimental term values, neglect-
247 ing Fermi resonance effects. Overall, the agreement is
248 surprisingly good, and the average deviation
249 ($\sim 9.9 \text{ cm}^{-1}$) is not much larger than the standard devi-
250 ation of the least squares treatment (8.1 cm^{-1}). Table 7
251 provides a complete list of the rovibronic transitions
252 that were fit in this work and the fit residuals.

253 4. Conclusions

254 We measured fluorescence excitation spectra of
255 fourteen bands with K'_a values of 0–2 in the
256 $\tilde{A}^2A_1 \leftarrow \tilde{X}^2B_1$ system of NH_2 . The spectra cover the re-

Table 6
Vibronic origins and residuals for the bands measured in this work

Band	Band origin (cm^{-1})	Observed – calculated (cm^{-1}) ^a
(0,16,0) Π	23 109.52	-15.08
(0,17,0) Δ	24 080.31	18.18
(0,17,0) Σ	24 094.27	7.86
(0,18,0) Π	25 049.19	-5.24
(0,19,0) Δ	26 003.56	-3.28
(0,19,0) Σ	26 052.63	2.18
(0,20,0) Π	27 024.84	-9.19
(0,21,0) Δ	27 978.43	-20.96
(0,21,0) Σ	28 039.83	-8.89
(0,22,0) Π	29 036.13	-7.13
(0,23,0) Δ	30 000.87	6.55
(0,23,0) Σ	30 066.28	-9.08
(0,24,0) Π	31 086.18	-14.78
(0,25,0) Σ	32 115.71	-9.10

^a Calculated values from Jungen et al. [30].Table 7
Transitions included in the fits for each band and the fit residuals

Rotational transition $N'_{K'_a K'_c} \leftarrow N''_{K''_a K''_c}$	Observed wavenumber (cm^{-1})	Observed – calculated (cm^{-1})
$\tilde{A}(0, 16, 0)\Pi \leftarrow \tilde{X}(0, 0, 0)K_a = 0$		
$2_{12} \leftarrow 2_{02} (F_1)$	23 095.60	0.75
$1_{11} \leftarrow 1_{01} (F_1)$	23 095.81	-0.33
$2_{12} \leftarrow 2_{02} (F_2)$	23 097.59	-0.76
$1_{11} \leftarrow 1_{01} (F_2)$	23 102.28	0.34
$1_{10} \leftarrow 0_{00} (F_1)$	23 116.78	-0.17
$1_{10} \leftarrow 0_{00} (F_2)$	23 122.94	0.16
$\tilde{A}(0, 17, 0)\Delta \leftarrow \tilde{X}(0, 0, 0)K_a = 1$		
$2_{20} \leftarrow 2_{12} (F_1)$	24 029.37	-0.38
$2_{20} \leftarrow 2_{12} (F_2)$	24 038.88	-0.50
$2_{20} \leftarrow 1_{10} (F_1)$	24 061.86	-0.62
$2_{21} \leftarrow 1_{11} (F_1)$	24 068.25	1.01
$2_{20} \leftarrow 1_{10} (F_2)$	24 071.48	-0.52
$2_{21} \leftarrow 1_{11} (F_2)$	24 077.80	1.01
$3_{22} \leftarrow 2_{12} (F_1)$	24 098.94	-0.02
$3_{22} \leftarrow 2_{12} (F_2)$	24 106.01	0.02
$\tilde{A}(0, 17, 0)\Sigma \leftarrow \tilde{X}(0, 0, 0)K_a = 1$		
$1_{01} \leftarrow 2_{11} (F_2)$	24 029.15	0.02
$1_{01} \leftarrow 2_{11} (F_1)$	24 029.37	0.03
$0_{00} \leftarrow 1_{10} (F_2)$	24 057.46	-0.01
$0_{00} \leftarrow 1_{11} (F_1)$	24 057.73	-0.01
$1_{01} \leftarrow 1_{11} (F_2)$	24 080.80	-0.07
$1_{01} \leftarrow 1_{11} (F_1)$	24 081.16	0.06
$2_{02} \leftarrow 1_{10} (F_2)$	24 114.04	0.06
$2_{02} \leftarrow 1_{10} (F_1)$	24 114.17	-0.08
$3_{03} \leftarrow 2_{11} (F_2)$	24 125.61	-0.03
$3_{03} \leftarrow 2_{11} (F_1)$	24 125.88	0.04
$\tilde{A}(0, 18, 0)\Pi \leftarrow \tilde{X}(0, 0, 0)K_a = 0$		
$2_{12} \leftarrow 2_{02} (F_1)$	25 027.81	-0.14
$2_{12} \leftarrow 2_{02} (F_2)$	25 029.15	0.10
$1_{11} \leftarrow 1_{01} (F_1)$	25 034.84	0.00
$1_{11} \leftarrow 1_{01} (F_2)$	25 036.91	0.09
$1_{10} \leftarrow 0_{00} (F_1)$	25 059.91	-0.03
$1_{10} \leftarrow 0_{00} (F_2)$	25 061.82	-0.14
$2_{11} \leftarrow 1_{01} (F_1)$	25 081.02	0.16
$2_{11} \leftarrow 1_{01} (F_2)$	25 082.01	0.01
$3_{12} \leftarrow 2_{02} (F_1)$	25 102.75	-0.01
$3_{12} \leftarrow 2_{02} (F_2)$	25 103.49	-0.04
$\tilde{A}(0, 19, 0)\Delta \leftarrow \tilde{X}(0, 0, 0)K_a = 1$		
$2_{20} \leftarrow 1_{10} (F_1)$	25 984.92	-0.26
$2_{20} \leftarrow 1_{10} (F_2)$	25 986.75	-0.24
$2_{21} \leftarrow 1_{11} (F_1)$	25 990.26	0.28

Table 7 (continued)

Rotational transition $N''_{K'_a K'_c} \leftarrow N''_{K''_a K''_c}$	Observed wavenumber (cm^{-1})	Observed– calculated (cm^{-1})
$2_{21} \leftarrow 1_{11} (F_2)$	25 991.97	0.22
$3_{22} \leftarrow 2_{12} (F_1)$	26 010.24	-0.04
$3_{22} \leftarrow 2_{12} (F_2)$	26 011.63	0.04
$4_{23} \leftarrow 3_{13} (F_1)$	26 032.35	0.01
$4_{23} \leftarrow 3_{13} (F_2)$	26 033.58	-0.01
$\tilde{A}(0, 19, 0)\Sigma \leftarrow \tilde{X}(0, 0, 0)K_a = 1$		
$1_{01} \leftarrow 2_{11} (F_2)$	25 987.51	-0.06
$1_{01} \leftarrow 2_{11} (F_1)$	25 987.74	-0.04
$0_{00} \leftarrow 1_{10} (F_2)$	26 015.85	0.01
$0_{00} \leftarrow 1_{11} (F_1)$	26 016.11	0.02
$1_{01} \leftarrow 1_{11} (F_2)$	26 039.35	0.03
$1_{01} \leftarrow 1_{11} (F_1)$	26 039.57	0.02
$2_{02} \leftarrow 1_{10} (F_2)$	26 072.58	0.02
$2_{02} \leftarrow 1_{10} (F_1)$	26 072.85	0.02
$3_{03} \leftarrow 2_{11} (F_2)$	26 084.40	0.00
$3_{03} \leftarrow 2_{11} (F_1)$	26 084.59	-0.01
$\tilde{A}(0, 20, 0)\Pi \leftarrow \tilde{X}(0, 0, 0)K_a = 0$		
$1_{10} \leftarrow 2_{02} (F_2)$	26 974.15	0.05
$1_{10} \leftarrow 2_{02} (F_1)$	26 974.45	0.09
$2_{12} \leftarrow 2_{02} (F_2)$	27 003.84	-0.14
$2_{12} \leftarrow 2_{02} (F_1)$	27 004.32	0.17
$1_{11} \leftarrow 1_{01} (F_2)$	27 011.09	0.08
$1_{11} \leftarrow 1_{01} (F_1)$	27 011.09	-0.16
$1_{10} \leftarrow 0_{00} (F_2)$	27 036.16	-0.04
$1_{10} \leftarrow 0_{00} (F_1)$	27 036.38	-0.03
$2_{11} \leftarrow 1_{01} (F_2)$	27 057.03	-0.03
$2_{11} \leftarrow 1_{01} (F_1)$	27 057.21	0.00
$\tilde{A}(0, 21, 0)\Delta \leftarrow \tilde{X}(0, 0, 0)K_a = 1$		
$2_{20} \leftarrow 1_{10} (F_2)$	27 959.51	-0.76
$2_{20} \leftarrow 1_{10} (F_1)$	27 961.63	-0.52
$2_{21} \leftarrow 1_{11} (F_2)$	27 965.75	0.68
$2_{21} \leftarrow 1_{11} (F_1)$	27 967.63	0.72
$3_{22} \leftarrow 2_{12} (F_2)$	27 987.40	0.16
$3_{22} \leftarrow 2_{12} (F_1)$	27 987.85	-0.36
$4_{23} \leftarrow 3_{13} (F_2)$	28 010.83	-0.05
$4_{23} \leftarrow 3_{13} (F_1)$	28 011.06	0.14
$\tilde{A}(0, 21, 0)\Sigma \leftarrow \tilde{X}(0, 0, 0)K_a = 1$		
$1_{01} \leftarrow 2_{11} (F_2)$	27 974.86	0.04
$1_{01} \leftarrow 2_{11} (F_1)$	27 975.09	0.07
$0_{00} \leftarrow 1_{10} (F_2)$	28 003.00	-0.04
$0_{00} \leftarrow 1_{11} (F_1)$	28 003.25	-0.05
$1_{01} \leftarrow 1_{11} (F_2)$	28 026.61	0.06
$1_{01} \leftarrow 1_{11} (F_1)$	28 026.77	-0.01
$2_{02} \leftarrow 2_{12} (F_2)$	28 027.08	-0.26
$2_{02} \leftarrow 2_{12} (F_1)$	28 027.32	-0.17
$3_{03} \leftarrow 3_{13} (F_2)$	28 031.01	-0.03
$3_{03} \leftarrow 3_{13} (F_1)$	28 031.17	0.01
$2_{02} \leftarrow 1_{10} (F_2)$	28 060.07	0.12
$2_{02} \leftarrow 1_{10} (F_1)$	28 060.44	0.22
$3_{03} \leftarrow 2_{11} (F_2)$	28 072.15	0.00
$3_{03} \leftarrow 2_{11} (F_1)$	28 072.38	0.03
$\tilde{A}(0, 22, 0)\Pi \leftarrow \tilde{X}(0, 0, 0)K_a = 0$		
$1_{10} \leftarrow 2_{02} (F_2)$	28 985.23	-0.15
$1_{10} \leftarrow 2_{02} (F_1)$	28 986.34	0.07
$2_{12} \leftarrow 2_{02} (F_2)$	29 015.50	0.11
$2_{12} \leftarrow 2_{02} (F_1)$	29 015.68	-0.22
$1_{11} \leftarrow 1_{01} (F_2)$	29 022.14	0.28
$1_{11} \leftarrow 1_{01} (F_1)$	29 022.73	0.00
$1_{10} \leftarrow 0_{00} (F_2)$	29 047.31	-0.17

Table 7 (continued)

Rotational transition $N''_{K'_a K'_c} \leftarrow N''_{K''_a K''_c}$	Observed wavenumber (cm^{-1})	Observed– calculated (cm^{-1})
$1_{10} \leftarrow 0_{00} (F_1)$	29 048.35	0.04
$3_{12} \leftarrow 2_{02} (F_2)$	29 093.59	-0.02
$3_{12} \leftarrow 2_{02} (F_1)$	29 094.05	0.07
$\tilde{A}(0, 23, 0)\Delta \leftarrow \tilde{X}(0, 0, 0)K_a = 1$		
$3_{21} \leftarrow 3_{13} (F_2)$	29 946.22	-0.09
$2_{20} \leftarrow 2_{12} (F_2)$	29 946.44	-0.07
$3_{21} \leftarrow 3_{13} (F_1)$	29 949.71	-0.31
$2_{20} \leftarrow 2_{12} (F_1)$	29 951.51	-0.17
$2_{20} \leftarrow 1_{10} (F_2)$	29 979.07	-0.05
$2_{21} \leftarrow 1_{11} (F_2)$	29 984.02	0.11
$2_{20} \leftarrow 1_{10} (F_1)$	29 984.56	0.15
$3_{21} \leftarrow 2_{11} (F_2)$	29 987.88	0.46
$2_{21} \leftarrow 1_{11} (F_1)$	29 989.19	0.02
$3_{21} \leftarrow 2_{11} (F_1)$	29 991.26	0.05
$3_{22} \leftarrow 2_{12} (F_2)$	30 001.38	-0.37
$3_{22} \leftarrow 2_{12} (F_1)$	30 005.75	0.26
$\tilde{A}(0, 23, 0)\Sigma \leftarrow \tilde{X}(0, 0, 0)K_a = 1$		
$1_{01} \leftarrow 2_{11} (F_2)$	30 007.06	-0.34
$1_{01} \leftarrow 2_{11} (F_1)$	30 007.40	-0.21
$0_{00} \leftarrow 1_{10} (F_2)$	30 035.43	0.00
$0_{00} \leftarrow 1_{11} (F_1)$	30 035.70	0.00
$1_{01} \leftarrow 1_{11} (F_2)$	30 059.46	0.32
$1_{01} \leftarrow 1_{11} (F_1)$	30 059.59	0.22
$3_{03} \leftarrow 3_{13} (F_2)$	30 063.67	-0.48
$3_{03} \leftarrow 3_{13} (F_1)$	30 064.35	0.08
$3_{03} \leftarrow 2_{11} (F_2)$	30 105.17	0.48
$3_{03} \leftarrow 2_{11} (F_1)$	30 105.94	-0.09
$\tilde{A}(0, 24, 0)\Pi \leftarrow \tilde{X}(0, 0, 0)K_a = 0$		
$1_{10} \leftarrow 2_{02} (F_2)$	31 035.58	-0.12
$1_{10} \leftarrow 2_{02} (F_1)$	31 035.90	-0.24
$2_{12} \leftarrow 2_{02} (F_2)$	31 069.48	-0.22
$2_{12} \leftarrow 2_{02} (F_1)$	31 070.25	0.28
$1_{11} \leftarrow 1_{01} (F_2)$	31 073.34	0.09
$1_{11} \leftarrow 1_{01} (F_1)$	31 073.41	-0.26
$2_{11} \leftarrow 1_{01} (F_2)$	31 121.30	0.42
$2_{11} \leftarrow 1_{01} (F_1)$	31 121.48	0.36
$3_{12} \leftarrow 2_{02} (F_2)$	31 145.78	-0.32
$3_{12} \leftarrow 2_{02} (F_1)$	31 146.29	-0.01
$\tilde{A}(0, 25, 0)\Sigma \leftarrow \tilde{X}(0, 0, 0)K_a = 1$		
$0_{00} \leftarrow 1_{10} (F_2)$	32 084.50	-0.37
$0_{00} \leftarrow 1_{11} (F_1)$	32 085.30	0.17
$1_{01} \leftarrow 1_{11} (F_2)$	32 109.10	0.19
$1_{01} \leftarrow 1_{11} (F_1)$	32 109.30	0.16
$3_{03} \leftarrow 3_{13} (F_2)$	32 119.50	0.14
$3_{03} \leftarrow 3_{13} (F_1)$	32 119.50	0.02
$2_{02} \leftarrow 1_{10} (F_2)$	32 143.80	-0.22
$2_{02} \leftarrow 1_{10} (F_1)$	32 144.30	0.02
$3_{03} \leftarrow 2_{11} (F_2)$	32 160.50	0.04
$3_{03} \leftarrow 2_{11} (F_1)$	32 160.50	-0.17

gion from 2900 to 4300 \AA , and include 10 bands not previously measured to our knowledge. Scattered rotational perturbations were observed but not analyzed in this work. The spectra are largely free from rotational perturbations at the low N values accessed in this experiment, and the molecular constants were obtained from a least squares fit to the determined spin-rovib-

257
258
259
260
261
262
263

264 ronic term values. The derived constants are in good
265 agreement with theoretical predictions incorporating the
266 effects of orbital angular momentum on the spin–rota-
267 tional fine structure.

268 Acknowledgments

269 The authors gratefully acknowledge partial support
270 of this work by the National Science Foundation under
271 Grant CHE-972803.

272 References

- 273 [1] G. Herzberg, D.A. Ramsay, *J. Chem. Phys.* 20 (1952) 347.
274 [2] K. Dressler, D.A. Ramsay, *J. Chem. Phys.* 27 (1957) 971–972.
275 [3] K. Dressler, D.A. Ramsay, *Philos. Trans. R. Soc. London Ser. A*
276 251 (1959) 553–602.
277 [4] J.P. Halpern, G. Hancock, M. Lenzi, K.H. Welge, *J. Chem. Phys.*
278 63 (1975) 4808–4816.
279 [5] G.W. Hills, D.L. Philen, R.F. Curl Jr., F.K. Tittel, *Chem. Phys.*
280 12 (1976) 107–111.
281 [6] J.W.C. Johns, D.A. Ramsay, S.C. Ross, *Can. J. Phys.* 54 (1976)
282 1804–1814.
283 [7] G.W. Hills, J.M. Cook, R.F. Curl Jr., F.K. Tittel, *J. Chem. Phys.*
284 65 (1976) 823–828.
285 [8] G.W. Hills, R.F. Curl Jr., *J. Chem. Phys.* 66 (1977) 1507–1513.
286 [9] J.M. Cook, G.W. Hills, R.F. Curl Jr., *J. Chem. Phys.* 67 (1977)
287 1450–1461.
288 [10] R.N. Dixon, D. Field, *Mol. Phys.* 34 (1977) 1563–1576.
289 [11] R.S. Lowe, J.V.V. Kasper, G.W. Hills, W. Dillenschneider, R.F.
290 Curl Jr., *J. Chem. Phys.* 70 (1979) 3356–3361.
291 [12] G.W. Hills, C.R. Brazier, J.M. Brown, J.M. Cook, R.F. Curl Jr.,
292 *J. Chem. Phys.* 76 (1982) 240–252.
293 [13] T. Amano, K. Kawaguchi, M. Kakimoto, E. Hirota, *J. Chem.*
294 *Phys.* 77 (1982) 159–167.
295 [14] S. Mayama, S. Hiraoka, K. Obi, *J. Chem. Phys.* 80 (1984) 7–12.
296 [15] K. Kawaguchi, T. Suzuki, S. Saito, E. Hirota, *J. Opt. Soc. Am. B*
297 4 (1987) 1203–1211.
298 [16] B. Hemmerling, M. Vervloet, *Chem. Phys. Lett.* 150 (1988) 464–
299 468.
300 [17] M. Vervloet, *Mol. Phys.* 63 (1988) 433–449.

- [18] S.C. Ross, F.W. Birss, M. Vervloet, D.A. Ramsay, *J. Mol.*
301 *Spectrosc.* 129 (1988) 436–470. 302
[19] A.R.W. McKellar, M. Vervloet, *J. Mol. Spectrosc.* 142 (1990)
303 319–335. 304
[20] R.N. Dixon, S.J. Irving, J.R. Nightingale, M. Vervloet, *J. Chem.*
305 *Soc. Faraday Trans.* 87 (1991) 2121–2133. 306
[21] J. Schleipen, J.J. ter Meulen, L. Nemes, M. Vervloet, *Chem. Phys.*
307 *Lett.* 197 (1992) 165–170. 308
[22] C.-H. Chang, S.-C. Lin, Y.-T. Chen, *J. Mol. Spectrosc.* 169 (1995)
309 427–439. 310
[23] J.J. Alwan, G.J. Eden, *Chem. Vapor. Depos.* 3 (1997) 209–217. 311
[24] H. Kawakita, K. Ayani, T. Kawabata, *Publ. Astron. Soc. Jpn.* 52
312 (2000) 925–930. 313
[25] J.A. Pople, H.C. Longuet-Higgins, *Mol. Phys.* 1 (1958) 372–
314 383. 315
[26] R.N. Dixon, *Mol. Phys.* 9 (1965) 357–366. 316
[27] S. Bell, H.F. Schaefer III, *J. Chem. Phys.* 67 (1977) 5173–
317 5177. 318
[28] S.D. Peyerimhoff, R.J. Buenker, *Can. J. Chem.* 57 (1979) 3182–
319 3189. 320
[29] Ch. Jungen, A.J. Merer, *Mol. Phys.* 40 (1980) 1–23. 321
[30] Ch. Jungen, K.-E.J. Hallin, A.J. Merer, *Mol. Phys.* 40 (1980) 25–
322 63. 323
[31] Ch. Jungen, K.-E.J. Hallin, A.J. Merer, *Mol. Phys.* 40 (1980) 65–
324 94. 325
[32] G. Duxbury, R.N. Dixon, *Mol. Phys.* 43 (1981) 255–274. 326
[33] R.P. Saxon, B.H. Lengsfeld III, B. Liu, *J. Chem. Phys.* 78 (1983)
327 312–320. 328
[34] M. Peric, S.D. Peyerimhoff, R.J. Buenker, *Mol. Phys.* 49 (1983)
329 379–400. 330
[35] H. Nakatsuji, M. Izawa, *J. Chem. Phys.* 97 (1992) 435–439. 331
[36] W. Gabriel, G. Chambaud, P. Rosmus, S. Carter, N.C. Handy,
332 *Mol. Phys.* 81 (1994) 1445–1461. 333
[37] R. Vetter, L. Züllicke, A. Koch, E.F. van Dishoeck, S.D.
334 Peyerimhoff, *J. Chem. Phys.* 104 (1996) 5558–5571. 335
[38] E.-Y. Feng, Z.-F. Cui, X.-Z. Zhao, D. Chen, Yuanzi Yu Fenzi
336 *Wuli Xuebao* 16 (1999) 369–374. 337
[39] Z.-F. Cui, D. Chen, E.-Y. Feng, T.-X. Lu, X.-C. Li, Yuanzi Yu
338 *Fenzi Wuli Xuebao* 17 (2000) 331–338. 339
[40] A. Alijah, G. Duxbury, *J. Mol. Spectrosc.* 211 (2002) 7–15. 340
[41] A. Alijah, G. Duxbury, *J. Mol. Spectrosc.* 211 (2002) 16–30. 341
[42] G. Duxbury, A. Alijah, *J. Mol. Spectrosc.* 211 (2002) 31–57. 342
[43] P. Jensen, T.E. Odaka, W.P. Kraemer, T. Hirano, P.R. Bunker,
343 *Spectrochim. Acta A* 58 (2002) 763–794. 344
[44] E. Hill, J.H. van Vleck, *Phys. Rev.* 32 (1928) 250–272. 345